Research article

Shulei Li, Mingcheng Panmai, Shaolong Tie, Yi Xu, Jin Xiang and Sheng Lan*

Regulating disordered plasmonic nanoparticles into polarization sensitive metasurfaces

https://doi.org/10.1515/nanoph-2020-0651
Received December 11, 2020; accepted January 31, 2021;
published online February 15, 2021

Abstract: Metasurfaces composed of regularly arranged and deliberately oriented metallic nanoparticles can be employed to manipulate the amplitude, phase and polarization of an incident electromagnetic wave. The metasurfaces operating in the visible to near infrared spectral range rely on the modern fabrication technologies which offer a spatial resolution beyond the optical diffraction limit. Although direct laser writing is an alternative to the fabrication of nanostructures, the achievement of regular nanostructures with deep-subwavelength periods by using this method remains a big challenge. Here, we proposed and demonstrated a novel strategy for regulating disordered plasmonic nanoparticles into nanogratings with deep-subwavelength periods and reshaped nanoparticles by using femtosecond laser pulses. The orientations of the nanogratings depend strongly on the polarization of the femtosecond laser light. Such nanogratings exhibit reflection and polarization control over the reflected light, enabling the realization of polarization sensitive optical memory and color display with high spatial resolution and good chromacity.

Keywords: color display; femtosecond laser pulse; gold nanoparticle; nanograting; optical memory; polarization control.

1 Introduction

Wavelength and polarization are two important parameters that characterize the physical properties of an electromagnetic wave or light. While the former comprises the information of photon energy and oscillation period of electric field, the latter gives the orientation of electric field in space. Basically, the information for the wavelength and polarization of a laser beam can be obtained by using a wavelength meter and a polarization analyzer. On the other hand, footprints of the laser wavelength and polarization of a laser beam can also be found in a material that interacts with the laser beam. A typical example is the so called laser-induced periodic surface structures (LIPSS) that are commonly observed on the surface of a material irradiated by using a pulsed laser beam, a phenomenon that has attracted intensive and extensive studies in the last three decades [1–4]. In general, LIPSSs look like gratings and may exhibit structural colors [5–7]. They are usually classified into low-frequency LIPSSs with a period close to the wavelength of the irradiated laser light and high-frequency LIPSSs with a subwavelength period much smaller than the laser wavelength [8–11]. So far, various physical mechanisms have been proposed to interpret the formation of low- and high-frequency LIPSSs on different materials [12–14]. It is remarkable, however, that in most cases low-frequency LIPSSs are perpendicular to the polarization of the irradiated laser light while high-frequency LIPSSs are parallel to the laser polarization. This behavior implies that the polarization state (we consider linear polarization in this work) of laser light can be imprinted on the surface of a material in the form of LIPSSs. Apparently, only high-frequency LIPSSs can be exploited to realize polarization imprinting with a subwavelength spatial resolution [15].

Shulei Li and **Mingcheng Panmai** contributed equally to this work.

***Corresponding author: Sheng Lan**, Guangdong Provincial Key Laboratory of Nanophotonic Functional Materials and Devices, School of Information and Optoelectronic Science and Engineering, South China Normal University, Guangzhou 510006, China,
E-mail: slan@scnu.edu.cn
Shulei Li and Mingcheng Panmai, Guangdong Provincial Key Laboratory of Nanophotonic Functional Materials and Devices, School of Information and Optoelectronic Science and Engineering, South China Normal University, Guangzhou 510006, China.
https://orcid.org/0000-0001-9346-3773 (S. Li)
Shaolong Tie, School of Chemistry, South China Normal University, Guangzhou 510006, China
Yi Xu, Department of Electronic Engineering, College of Information Science and Technology, Jinan University, Guangzhou 510632, China
Jin Xiang, Department of Electrical and Computer Engineering, University of Wisconsin–Madison, Madison, WI, USA.
https://orcid.org/0000-0003-0896-7526

Thin films of noble metal, such as gold (Au) or silver (Ag), generally exhibit broad reflection spectra. It has been known that the broad reflection spectrum of a metal film can be dramatically modified to exhibit vivid structural colors by adding an array of metallic nanoparticles on top of the meal film (usually separated by a dielectric spacer layer) [16–19], forming the so-called particle-on-film system. Moreover, color printing can be realized by laser-induced reshaping of the metallic nanoparticles [20]. The reflection spectrum of such a particle-on-film system may exhibit a dependence on the polarization of the incident light if the shape of the nanoparticles is asymmetric [21–23], such as nanorods [24, 25], nanogrooves [26, 27], and nanogratings [28, 29]. In these cases, a polarization sensitive color display can be achieved. It is noticed, however, that sophisticated facilities (such as electron beam lithography and reactive ion etching), complicated procedures and accurate control are necessary to produce plasmonic metasurfaces composed of regular arrangements of nanoparticles with specified size, shape, and orientation [30–32]. The thickness of the spacer layer in the particle-on-film system also plays a crucial role in the interaction of the regular/random array of plasmonic nanoparticles with femtosecond laser light [33–35]. Moreover, a soft spacer layer (e.g., a polymer film) rather than a hard one (e.g., silica) is quite important for the reshaping and regulation of nanoparticles [36–38], as demonstrated in this work. Apart from perfect absorption and vivid structural colors demonstrated in previous studies by exploiting a variety of particle-on-film systems (or various combinations of a metasurfaces and a thin metal film) [39–43], the applications of such plasmonic metasurfaces in polarization control and optical data storage have also attracted great interest in recent years, such as polarization controlled high-resolution grayscale image display and multiplexed anti-counterfeiting meta-image display with single-sized nanostructures [44, 45].

Previously, the reflection properties of a hybrid structure composed of a lossy dielectric layer and a metal film was investigated [33, 34]. It was found that the phase of the reflected light depends on the complex refractive indices of the two materials and it can take the place of the phase accumulated via propagation through a thicker layer [33]. For this reason, this structure allows for suppression of reflectivity (enhanced absorption) through destructive interference of all of the reflected partial waves, leading to vivid structural colors that are quite sensitive to the thickness of the lossy dielectric layer. In principle, the reflection properties of a particle-on-film system can be understood by using the thin film interference theory described above. Here, the regular/random array of particles acts as a lossy material and the spacer layer in between provides an additional phase accumulation which depends on its thickness. The reflection spectrum of the particle-on-film system is ultimately governed by the interference of all the reflected partial waves. Very recently, the physical mechanism for modifying the reflection spectrum of a particle-on-film system with the thickness of the spacer layer was interpreted based on the coupled model theory [35]. In this model, the spacer layer acts as an external optical cavity that supports an optical mode whose resonant wavelength can be adjusted by its thickness. The reflection spectrum of the particle-on-film system is determined by the coupling efficiency between the plasmon modes supported by the nanoparticle array and the external optical cavity (i.e., the spacer layer). Therefore, vivid structural colors originating from the phase transition from the broadband absorption to limited band reflection can be achieved by simply varying the thickness of the spacer layer. Apparently, the modification of the reflection spectrum for such a particle-on-film system can also be realized by regulating the plasmon modes of the nanoparticle array through laser ablation, which is more convenient and useful from the viewpoint of practical application.

In this article, we investigated the interaction of a particle-on-film system, in which the nanoparticles are closely packed and the thickness of the spacer layer is deliberately designed, with femtosecond laser pulses. We observed the formation of nanograting with deep-subwavelength periods through the regulation of disordered nanoparticles with high-power laser pulses. We showed that the nanogratings exhibit polarization control over the reflected light, which implying potential applications in high-density optical memory and polarization sensitive optical display.

2 Methods

2.1 Sample preparation

The samples used in our experiments were fabricated by three steps. First, Au films with a thickness of ~100 nm were deposited on silica (SiO_2) substrates by sputtering. Then, PMMA films of different thicknesses were spin-coated on Au/SiO_2 substrates. Finally, two-dimensional closely-packed Au nanoislands were deposited on the surfaces of PMMA films by sputtering. The morphology of closely-packed Au nanoislands could be controlled by the sputtering time and it was set to be ~30 s in our experiments.

2.2 Experimental setup

The femtosecond laser light with a repetition rate of 76 MHz and a duration of 130 fs was employed to irradiate the closely-packed Au

nanoislands created on the surfaces of PMMA films. The femtosecond laser light was focused on the samples by using the 60× objective lens (NA = 0.85) of an inverted microscope (Axio Observer A1, Zeiss). The samples were placed on a three-dimensional positioning system with an accuracy of 1.0 nm in all dimensions (P-563.3CD, Physik Instruments) which was driven by a piezoelectric ceramic. The recoding of patterns was carried out by moving the samples. A mechanical shutter was employed to control the irradiation time of the femtosecond laser pulses, which was set to be 10 ms in our case. Limited by the expansion range of the piezoelectric ceramic, the maximum moving area of the positioner is $300 \times 300\ \mu m^2$. This is the largest area for the pattern we could record. In this work, we used a halogen lamp with or without a polarizer as the illumination white light source. The reflection light from a specified area was collected by using the same objective lens and directed to a spectrometer (SR-500i-B1, Andor) for analysis or to a coupled-charge device (DU970 N, Andor) for recording.

2.3 Numerical model

The reflection spectra of the samples with different configurations were calculated numerically based on the finite element method (FEM) by using a commercially developed software (COMSOL Multiphysics v5.4) or the finite-difference time-domain (FDTD) method by using a using a commercially developed software (FDTD solution).

The numerical simulations using the FEM method were performed in a sphere whose diameter was set to be the wavelength of the incident light. The sample was placed at the center of the sphere which was enclosed by a periodic boundary condition. For the numerical simulations using the FDTD method, we employed a plane wave to evaluate the reflectivity of the sample. The smallest mesh size was chosen to be 1.0 nm in order to obtain converged simulation results and periodic boundary condition was employed to terminate the finite simulation region.

3 Results and discussion

3.1 Nanogratings induced by femtosecond laser pulses

Figure 1A shows the structural color exhibited by a particle-on-film composed of a non-uniform polymer (PMMA) film sandwiched by two Au films. The bottom Au film deposited on a silica (SiO_2) substrate was a flat one with a thickness of ~100 nm. The upper Au film was obtained by sputtering Au (~30 s) on the polymer film (see Supplementary Material, Figure S1), which was beforehand spin-coated on the bottom Au film. It consisted of closely-packed Au nanoislands, as schematically shown in Figure 1B. The average diameter and height of Au nanoislands were estimated to be ~50 and ~12 nm, respectively. If we consider the upper Au film as a lossy material, then the reflection spectrum of this particle-on-film system and thus the structural color is basically governed by the local thickness of the polymer (non-uniform), which determines the phase shift of the reflected partial waves [34]. Figure 1B illustrates schematically the morphology change of closely–packed Au nanoislands when the fluence of the femtosecond laser light is increased, which was confirmed later by scanning electron microscope (SEM) observation. In the initial stage, Au nanoislands are closely packed although their shapes (top view) appear to be much different (see phase i in Figure 1B). For a laser beam with specified wavelength and polarization, hot spots with enhanced electric field are expected to present owing to the plasmonic coupling between Au nanoislands. Femtosecond laser light interact preferentially with those Au nanoislands located around the hot spots, leading to the melting, deformation and even merge of these Au nanoislands. Another physical mechanism responsible for the melting and reshaping of Au nanoislands might be solid state dewetting [43, 46]. When closely-packed Au nanoislands are irradiated by using femtosecond laser light with a small fluence, some larger nanoparticles originating from the aggregation of small Au nanoislands were observed (see phase ii in Figure 1B). For femtosecond laser light with a moderate fluence, nearly all Au nanoislands are transformed into nanoparticles and become isolated from their neighbors. However, the shape of isolated Au nanoparticles is irregular and their distribution is random (see phase iii in Figure 1B). This situation is changed dramatically when femtosecond laser light with a large fluence is employed. In this case, most Au nanoparticles are reshaped into elliptical nanoparticles and arranged approximately into an ordered structure, forming a nanograting with a specified orientation (see phase iv in Figure 1B). More interestingly, the elongation direction of Au nanoparticles and the orientation of the nanograting are found to be perpendicular to the polarization of the femtosecond laser light.

The optical properties of the laser-induced nanogratings are schematically depicted in Figure 1C and D. These properties will be confirmed in the experimental results described in the following. As illustrated in Figure 1C, reflected light with different colors can be observed if the nanograting is illuminated with unpolarized white light and a polarization analyzer is rotated. Similar behavior is observed if polarized white light is used as illumination source and the polarization angle with respect to the vector of the nanograting (defined as the direction perpendicular to the orientation of the nanograting) is varied. Another intriguing property of the nanograting, which is schematically illustrated in Figure 1D, is the ability of manipulating the polarization state of the reflected light. When the polarization of the incident light is parallel or perpendicular to the vector of the nanograting, its polarization is preserved in the

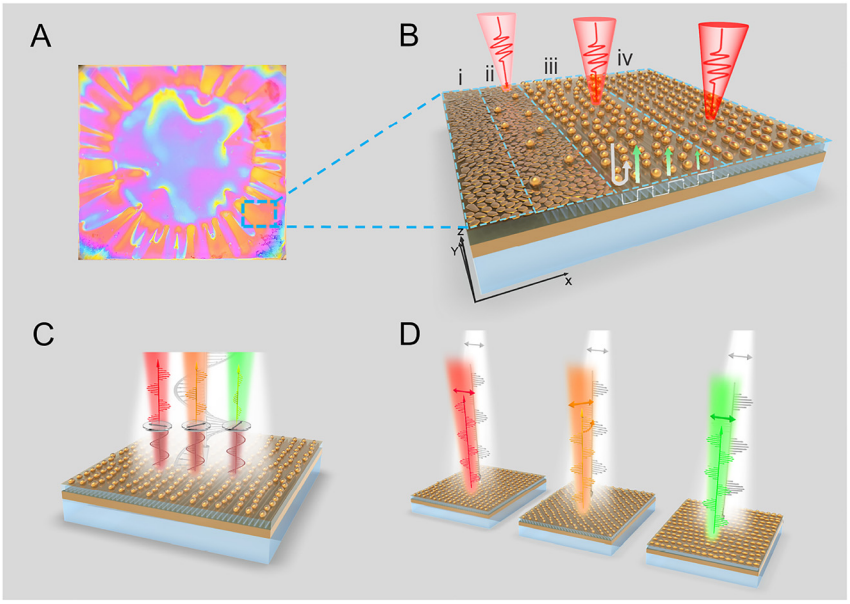

Figure 1: Regulating disordered plasmonic nanoparticles into nanogratings for polarization sensitive color display.
(A) Structural colors exhibited by disordered Au nanoparticles deposited on a non-uniform polymer (PMMA) film coated on a thin Au film. (B) Schematic showing the evolution of the disordered Au nanoparticles induced by increasing the laser fluence and the formation of a nanograting composed of regularly arranged elliptical Au nanoparticles. (C) Schematic showing the observation of different structural colors in the reflected light of a nanograting irradiated with unpolarized white light by rotating the polarization analyzer. (D) Schematic showing the preservation or rotation of the polarization state of the incident light in the reflected light, depending on the polarization angle of the incident light with respect to the vector of the nanograting.

reflected light. An obvious rotation of the polarization state of the incident light is observed when the angle between the polarization of the incident light and the vector of the nanograting exceeds 5°. More interestingly, the polarization of the reflected light can be completely rotated to the vector of the nanograting if the angle between the polarization of the incident light and the vector of the nanograting is close to 45°.

In our experiments, we first examined the evolution of two-dimensional closely-packed Au nanoislands upon the irradiation of femtosecond laser light with increasing fluence by SEM observations (see Supplementary Material, Figure S2). It is found that the evolution of the surface morphology follows exactly what we show schematically in Figure 1B. In Figure 2A, we present the evolution of the surface color (i.e., the color of the reflected light) with increasing laser fluence observed for incident white light with different polarization angles (α) of 0°, 30°, 60°, and 90°. Other examples for polarization sensitive structural colors are provided in Supplementary Material (see Supplementary Material, Figure S3). A significant change of the surface color is observed when the laser fluence is increased. However, it is noticed that the surface color, which is not sensitive to the polarization of the white light at low laser fluences, becomes highly polarization dependent at high laser fluences. In this case, the surface appears as red and green respectively under the illumination of white light with α = 0° and 90°.The derived color indices are plotted in a color diagram (CIE 1931) (see Supplementary Material, Figure S4). Apart from laser fluence, the surface color also exhibits a strong dependence on the laser wavelength (see Supplementary Material, Figure S5), especially at high laser fluences. More interestingly, black surface color (i.e., perfectly absorber in the visible light spectrum) is achieved at high laser fluences when the laser wavelength is chosen to be 850 nm. Since nanogratings composed of periodic arrangements of elongated Au nanoparticles are observed at high laser fluences, the surface color becomes highly sensitive to the polarization angle of the illuminating white light. The evolution of the reflection spectrum with increasing laser fluence measured for white light with polarization angles (α) of 0° and 90° are presented in Figure 2B (see Supplementary Material for the spectrum of the white light, Figure S6). It is noticed that the reflection spectra for α = 0° and α = 90° are dominated by reflection peaks at 750 and 550 nm, respectively. This unique feature plays a crucial role in the polarization control over the reflected light, as demonstrated in the following. For comparison, the simulated reflection spectra with increasing laser fluence are also provided (for

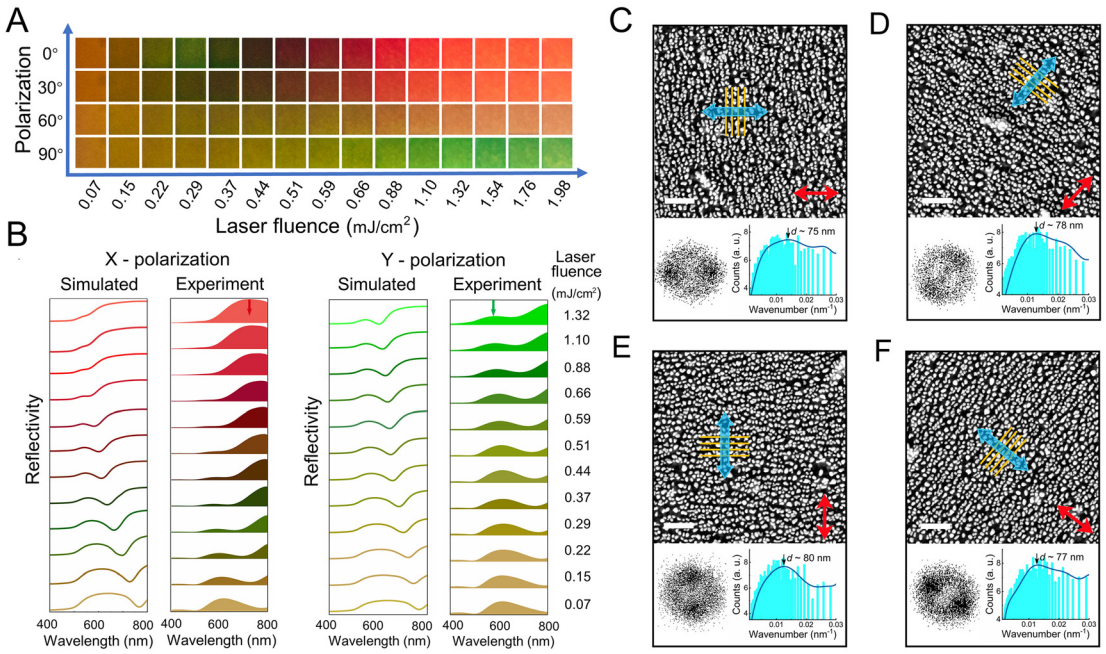

Figure 2: Polarization sensitive structural color and nanogratings created induced by femtosecond laser pulses with different fluences and polarizations.

(A) Tunable color palettes obtained by irradiating the sample surfaces with femtosecond laser pulses of different fluences and illuminated them with white light of different polarizations. (B) Reflection spectra measured and calculated for nanostructures induced by femtosecond laser pulses with different fluences and irradiated by using white light with polarization angles of 0° and 90°. The red and green arrows indicate the reflection peaks appearing in the reflection spectra of the nanogratings fabricated at high laser fluence and irradiated by using white light with polarization angles of 0° and 90°. SEM images of the nanogratings induced by using femtosecod laser light with polarization angles of 0° (C), 45° (D), 90° (E) and 135° (F), respectively. In each case, the orientation of the nanograting is indicated by paralleled yellow lines. The vector of the nanograting and the polarization of the laser light are marked by blue and red arrows, respectively. In addition, the Fourier transformation of the SEM image, which shows the orientation and period of the nanograting, is also provided as an inset. The length of the scale bar is 300 nm.

numerical simulation method, see Supplementary Material, Figure S7). In our model, we simulate the formation of elliptical Au nanoparticles by varying the long axis of the ellipsoid. In this case, the short axis is changed accordingly to keep the volume of the ellipsoid unchanged. Since Au nanoparticles are supported by a polymer film with a low melting point, Au nanoparticles reshaped by laser light might be partly embedded into the polymer film, as evidenced in the SEM observation (see Supplementary Material, Figure S8). This behavior is different from Au nanoparticles formed on hard substrates (e.g., a silica substrate) and the use of the soft polymer film has its own advantages in producing vivid structural colors, as demonstrated in this work. Although a simple physical model is used in numerical simulation, the simulation results capture the main features of the reflection spectra and agree qualitatively with the experimental observations (see Supplementary Material, Figure S7). In Figure 2B, it can be seen that the locations of the two reflection peaks and the evolution of the reflection spectrum can be reproduced by using the simple physical model described above. The difference between them arises mainly from the simple model in which a regular arrangement of identical Au nanoparticles is employed, which is not the real case.

In Figure 2C–F, we present the SEM images for the nanogratings generated by using femtosecond laser pulses with $\theta = 0°$, 45°, 90° and 135°. In each case, it is remarkable that both the elongation direction of Au nanoparticles and the orientation direction of the nanograting are perpendicular to the laser polarization. More clearly, the direction of the periodic arrangement of a nanograting, which is usually defined as the vector of the nanograting, can be revealed from the Fourier transformation of its SEM image. In addition, the period of the nanograting was extracted to be ~80 nm, which is only one-tenth of the laser wavelength (i.e., deep-subwavelength). The physical mechanism for the formation of such high-frequency LIPSSs is complicated, which cannot be predicted by using the theory proposed previously [8] (see Supplementary Material, Figure S9). Basically, the laser wavelength plays a crucial

role in determining the period of the nanograting. In this work, nanogratings with deep subwavelength periods are fabricated, which is only one-tenth of the laser wavelength. Since the tunable wavelength range of our femtosecond laser is 750–850 nm, it is difficult to discriminate the slight change in the period of the nanograting induced by laser pulses with different wavelengths. In addition, the interaction of Au nanoislands with femtosecond laser pulses depends strongly on the thickness of the polymer film, which determines the reflection (or absorption) of the femtosecond laser pulses. Apart from the nanogratings composed of elliptical Au nanoparticles, the formation of ripple-like nanogratings was also observed in the underlying polymer film (see Supplementary Material, Figure S8). Similarly, the orientation of the ripples was also found to be perpendicular to the laser polarization and the period of the nanograting was estimated to be ~80 nm.

3.2 Polarization control over reflected light for optical memory

The most intriguing and important optical property of the laser-induced nanogratings is the polarization control over the reflected light. We experimentally measured the polarization states of the horizontally-polarized white light ($\alpha = 0°$) reflected from the nanogratings fabricated by using femtosecond laser pulses with different polarization angles (θ = 0°, 45°, 90° and 135°). The polarization states of the reflected light are presented in Figure 3A–D for long wavelengths and Figure 3E–H for short wavelengths, respectively. The orientations of the nanogratings and the polarization of the incident white light are shown in the insets. Obviously, the angles between the vectors of the nanogratings and the polarization of the white light are found to be 0°, 45°, 90° and 135°, respectively.

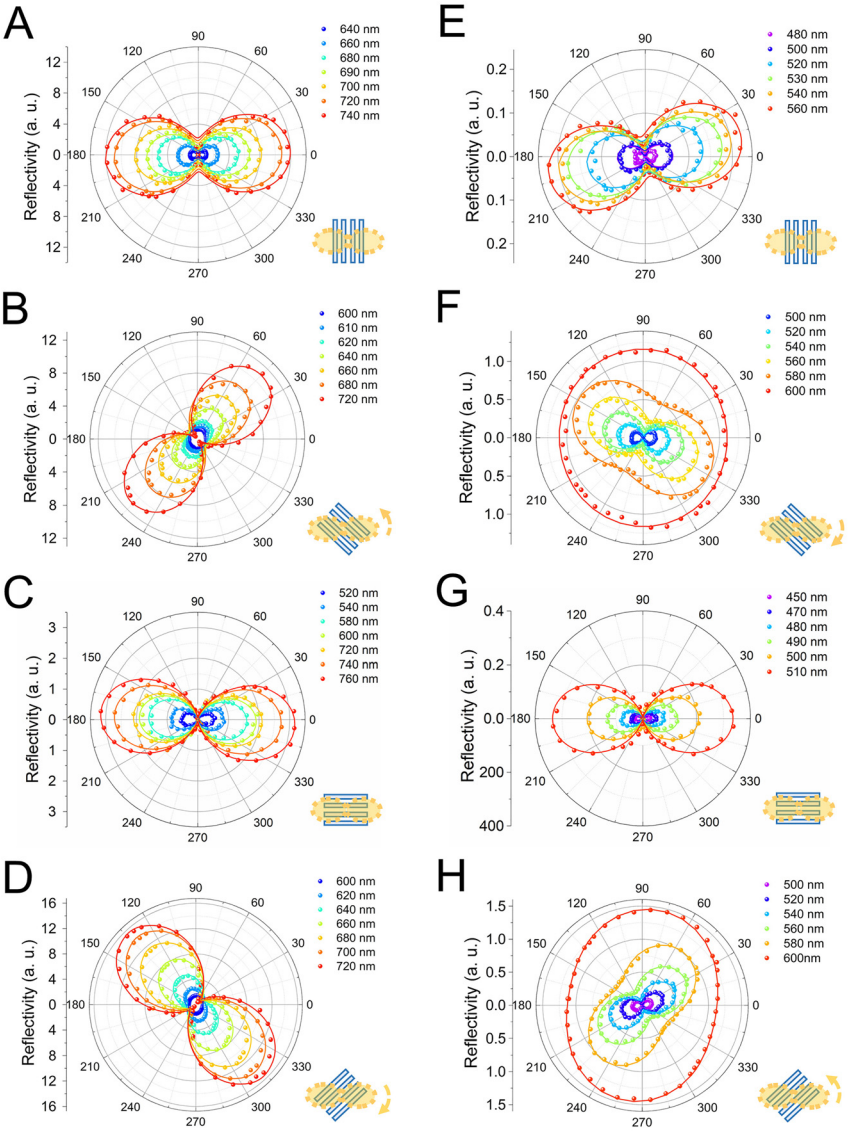

Figure 3: Polarization control over the reflected light of nanogratings. (A, E) Nanogratings by using femtosecond laser pulses with θ = 0° and irradiated by using white light with α = 0°. (B, F) Nanogratings by using femtosecond laser pulses with θ = 45° and irradiated by using white light with α = 0°. (C, G) Nanogratings by using femtosecond laser pulses with θ = 90° and irradiated by using white light with α = 0°. (D, H) Nanogratings by using femtosecond laser pulses with θ = 135° and irradiated by using white light with α = 0°. In each case, the orientation of the nanograting are presented in the inset.

Basically, the incident light with an arbitrary polarization angle can be decomposed into the two components parallel ($\alpha = 0°$) and perpendicular ($\alpha = 90°$) to the vector of the nanograting. As shown in Figure 2B, the reflection peaks appearing at 750 and 550 nm for incident light with $\alpha = 0°$ and $\alpha = 90°$ correspond to the radiations of the two plasmon modes excited in the nanograting. For incident light with $\alpha = 0°$ or $\alpha = 90°$, only the parallel or the perpendicular plasmon mode will be excited in the nanograting. As a result, the polarization state of the incident light is preserved and it is independent of wavelength, as shown in Figure 3A, C, E and G. For incident light with an arditrary polarization angle, the polarization state of the reflected light is determined by the interference of the radiations from the two plasmon modes with a phase difference [47]. In this case, the polarization state of the reflected light exhibits a strong dependence on wavelength (λ), as shown in Figure 3B, D, F and H. For incident light with $\alpha = 45°$, the polarization state at $\lambda = 500$ nm is the same as that of the incident light (i.e., linear polarization with $\alpha = 0°$). With increasing wavelength, however, a rotation of the polarization state towards the nanograting (or an increase of the polarization angle) is observed. One can see an elliptical polarization at $\lambda = 580$ nm and an circular polarization at $\lambda = 600$ nm (see Figure 3F). The circular polarization is changed to an elliptical one at $\lambda = 620$ nm. After that, a rotation of the polarization state is observed again with increasing wavelength. Finally, a linear polarization state along the vector of the nanograting is obtained at $\lambda = 720$ nm (see Figure 3B). This behavior can be easily understood if one notices that the amplitude of the parallel plasmon mode is much stronger than that of the perpendicular one owing to the grating effect (see Figure 2B). When the polarization angle deviates from 0° and 90°, a rotation of the polarization state toward the vector of the nanograting is observed (see Supplementary Material, Figure S10).

Actually, the polarization state of the reflected light is governed by the parallel plasmon mode. This is the reason why the polarization state of the reflected light at long wavelengths is always rotated towards the vector of the nanograting and why it can be rotated almost to the vector of the nanograting when the polarization angle of the incident light is close to 45° or 135° (Figure 3B, D, F and H). From the viewpoint of practical application, the nanogratings like this can be employed to realize efficient polarization rotation and conversion (e.g., from linear to elliptical or circular polarization).

The unique feature of laser-induced nanogratings described above offers us the opportunity for imprinting the laser polarization states as nanogratings with high spatial and angle resolutions. The readout of the imprinted polarization states can be realized by exploiting the polarization maintaining and rotating behavior of the nanogratings. In Figure 4A, we demonstrated the recording and readout of the laser polarization state in a chain of characters (Science & Technology). From left to right, each character is recorded by using femtosecond laser pulses with an increased polarization angle of 10°, starting from $\theta = 0°$. In order to identify the recorded polarization state, we employed the combination of a polarizer and a analyzer with cross polarization (i.e., the angle between the

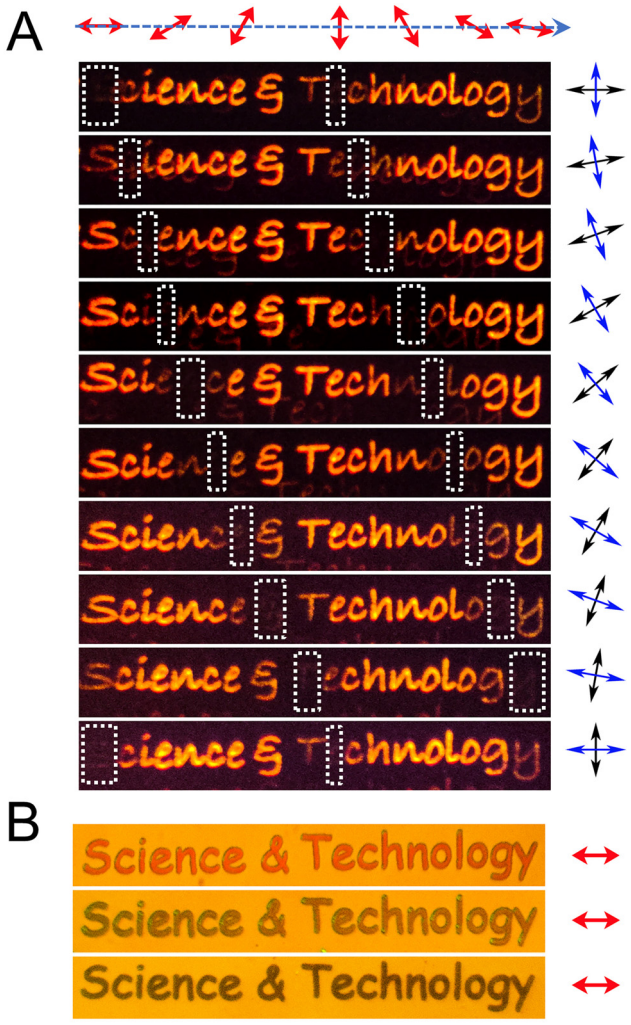

Figure 4: Optical memory realized by using nanogratings. (A) Recording of characters "Science & Technology" by using femtosecond laser pulses with an increasement of 10° in polarization angle. The readout of the recorded polarization states was achieved by using the combination of a polarizer and a analyzer with cross-polarization. (B) Recording of characters "Science & Technology" by using femtosecond laser pulses with the same polarization (horizontal) and power but with different wavelengths of 750, 800 and 850 nm.

polarizer and the analyzer was kept to be 90°, as indicated on the right side). Since the polarization state can only be prevented for nanogratings whose vectors are parallel or perpendicular to the polarization of the incident light, only the characters imprinted with such nanogratings will disappear when the polarizer/analyzer was rotated. As can be seen in Figure 4A, the characters in the chain disappeared sequentially when the polarizer/analyzer was rotated to 0°, 10°, 20°, 30°, 40°, 50°, 60°, 70°, 80°, implying the realization of 10° angle resolution for the polarization state. The characters were recorded by using a pixel size of 0.7 μm and the narrowest part of each character contains only one pixel. It means the laser polarization state can be imprinted with a spatial resolution close to 0.7 μm. Actually, the spatial resolution can be further improved to 0.5 μm (see Supplementary Material, Figure S11). In Figure 4B, we show that different laser wavelengths with the same polarization can be recorded as different surface colors (see Supplementary Material, Figure S5). By combining nine polarization states and three wavelengths of the laser light, one can record $9 \times 3 = 27$ different states with a pixel size as small as $0.5 \times 0.5\ \mu m^2$, implying the possibility for realizing optical memory with an ultrahigh density.

3.3 Polarization sensitive color display realized by nanogratings

The formation of nanogratings composed of elliptical Au nanoparticles implies the strong dependence of the reflected light, including its spectrum and polarization state, on the polarization of the incident light. These unique features can be exploited to realize polarization sensitive color display. In order to show polarization sensitive color display realized by using the laser-induced nanogratings, we designed a pattern comprising colorful flowers and leaves and imprinted it on the sample by using femtosecond laser pulses with different wavelengths, polarizations and fluences, as shown in Figure 5A (for the detailed parameters, see Supplementary Material, Figure S12). Under the illumination of unpolarized white light, only tedious colors (black and brown) can be observed. In sharp contrast, abundant structural colors, including red, green, yellow, orange, brown and black etc., are presented if the pattern is illuminated by using linearly polarized white light. Particularly, these colors are quite sensitive to the polarization of the irradiated white light, as shown in Figure 5A, where the evolution of the colored patten with increasing polarization angle of the white light is presented (see Supplementary Material, Figure S13).

As described above, the designed pattern exhibits polarization sensitive colors owing to the existence of laser-induced nanogratings. The reflection spectrum of a specified area depends strongly on the angle between the imprinted nanograting and the polarization of white light. In Figure 5B,C we show another two intriguing features observed for laser-induced nanogratings. If a pattern is illuminated with unpolarized white light and observed after a polarization analyzer, it appears exactly the same as that observed by using white light with the same polarization angle, as shown in Figure 5B, where the school logo is examined after a polarization analyzer with ϕ = 0°, 30°, 60° and 90°. As can be seen in Figure 5A, some colors (e.g., purple and pink) in the designed pattern were not generated in the imprinted one. Apart from the laser wavelength, polarization and fluence, it was found that the thickness of the polymer film also plays a crucial role in the color generation (see Supplementary Material, Figure S14A). The surface colors described above are generated by using a PMMA film with a thickness of ~80 nm. When we reduced slightly the thickness of the PMMA film to 70 nm, we were able to produce some missing colors, as shown in Figure 5C. It was found that abundant colors can only be obtained by using polymer films with thicknesses ranging from 60 to 140 nm. If the thickness of the polymer film is smaller than 50 nm, no surface color is produced although the recorded pattern can be identified. Similarly, only green color is observed if the polymer film is thicker than 150 nm (see Supplementary Material, Figure S14B). In our case, the surface colors originate from the reflection of the incident white light from a particle-on-film system. It depends strongly on the phase difference between the refected partial waves, which is also related to the thickness of the polymer film [34, 35]. If we observe the scattering light instead of the reflected light by using an oblique incidence beam, the structural color will disappear (see Supplementary Material, Figure S15). It was also found that the structural color may also be affected by the pixel size used for recording the pattern (see Supplementary Material, Figure S16). When the pixel size becomes smaller than the laser spot size, overlap of neighboring laser spots occurs, leading to the reduction of the spatial resolution. It is equivalent to the increase of the laser fluence which leads to the disappearance of some details (such as the veins in the leaves). This is the reason why the pattern obtained by using 0.5 μm pixel size is not as good as that obtained by using 0.7 μm pixel size. In addition, it was confirmed that the nanograting formation and nanoparticle reshaping can only be realized by using femtosecond laser pulses rather than continuous wave laser light (see Supplementary Material, Figure S17).

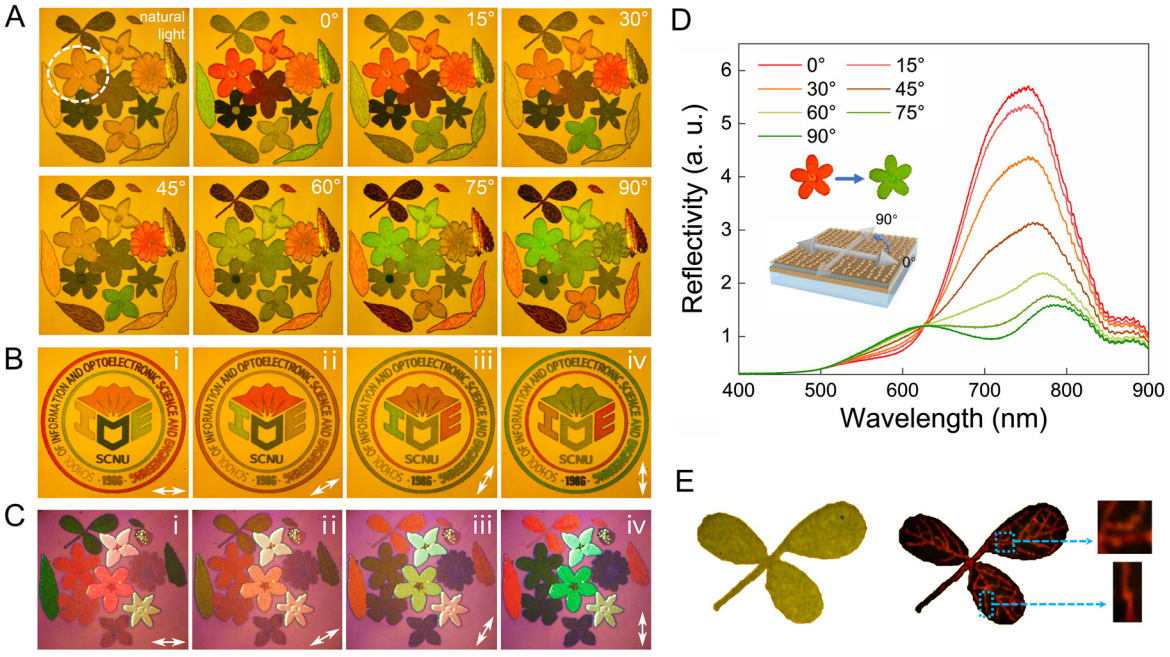

Figure 5: Polarization sensitive color display realized by using nanogratings.
(A) Microscope images of flowers and leaves observed by irradiating the pattern with un-polarized white light and white light with different polarization angles. (B) Microscope images obtained by irradiating the pattern with an unpolarized white light and observed after a polarization analyzer with different polarization angles of 0°, 30°, 60°, and 90° (i–iv). (C) Microscope images obtained under the same conditions in (D) for a sample with a 70 nm thick polymer film. (D) Reflection spectra measured for flower No. 7 (enclosed by dashed circle in (A)) which is irradiated with white light of different polarization angles with respect to the nanograting. 0° and 90° correspond to the white light whose polarizations parallel and perpendicular to the vector of the nanograting, as shown in the inset. (E) Leaf No. 1 observed under white light illumination with polarization angles of 0° (left) and 90° (right). The enlarged parts of the veins indicate a spatial resolution close to a pixel (~0.70 μm).

In Figure 5D, we show the dependence of the reflection spectrum on the polarization angle of the white light measured for a typical flower (flower No. 7). For $\alpha = 0°$, the spectrum is dominated by a strong reflection peak located at ~750 nm and the flower appears as red. With increasing polarization angle, the 750 nm peak is reduced and shifted to longer wavelengths. Meanwhile, a new reflection peak emerged at a shorter wavelength. Finally, two peaks located at ~620 and ~790 nm are observed in the reflection spectrum and the flower becomes green at $\alpha = 90°$ (see the inset in Figure 5D). For nanogratings fabricated by using 750 nm femtosecond laser pulses, they generally appear as red when exposed to white light whose polarization is parallel to the vector of the nanogratings. The red color is changed to green for white light with polarization perpendicular to the vector of the nanogratings. The red and green colors (i.e., the resonant wavelengths) corresponding to $\alpha = 0°$ and 90° respectively represent the two basic plasmon modes of a nanograting. For white light with an arbitrary polarization angle ($0° < \alpha < 90°$), these two basic modes are excited simultaneously and the reflected light is determined by the interference of their radiations [39]. A more interesting phenomenon is found for the leaf No. 1, as shown in Figure 5E. The veins inside the leaf is invisible for white light with $\alpha = 0°$ owing to their similar color to that of the background. Surprisingly, they are clearly revealed when exposing to white light with $\alpha = 90°$ because of the large contrast in color with the background, although both colors are dramatically changed. It should be emphasized that the thinnest part of the veins (~700 nm) inside the leaf is close to the optical diffraction limit (see the enlarged images in Figure 5E).

In this work, we are dealing with the interaction of Au nanoislands with femtosecond laser pulses, which lead to the formation of nanogratings (a kind of LIPSS). Based on previous studies, the formation of LIPSSs generally requires high-peak powers which are available only in femtosecond laser pulses. In addition, reshaping of nanoparticles also depends strongly on the peak power of pulse lasers [48]. For this reason, we think that the similar results, i.e., the nanogratings described in this work cannot be achieved by using nanosecond laser pulses.

4 Conclusions

In summary, we have proposed and demonstrated a novel strategy for regulating disordered plasmonic nanoparticles into nanogratings with deep-subwavelength periods and reshaped nanopartucles by exploiting the interaction of two-dimensional closely-packed Au nanoislands with femtosecond laser pulses. The orientation direction of the nanograting and the elongation direction of the Au nanoparticles were found to be perpendicular to the laser polarization. The reflected light exhibited different colors depending on the laser polarization, wavelength and power. Nanogratings exhibit polarization control over the reflected light, depending strongly on the angle between the nanograting and the polarization of the incident light. This unique feature was employed to record and readout laser polarization with an angle resolution of 10° and a spatial resolution of ~0.5 μm. Polarization sensitive color display was also realized by using nanogratings generated at high laser fluences. As compared with the sophisticate technologies used to fabricate plasmonic metasurfaces, such as the combination of electron beam lithography and reactive ion etching, the method proposed in this wok has the advantages of easy fabrication and cost effective. Moreover, our findings provide a new method for generating plasmonic nanograting and pave the way for realizing ultrahigh-density optical memory and polarization sensitive color display.

Author contributions: All the authors have accepted responsibility for the entire content of this submitted manuscript and approved submission.

Research funding: This research was financial support by National Key Research and Development Program of China (No. 2016YFA0201002), the National Nature and Science Foundation of China (Grant Nos. 11674110, 11874020 and 11674130), and the Natural Science Foundation of Guangdong Province, China (Grant No. 2016A030308010 and 2016A030306016). S. Li acknowledges the support from the Innovation Project of Graduate School of South China Normal University (No. 2019LKXM017).

Conflict of interest statement: The authors declare no conflicts of interest regarding this article.

References

[1] H. Van Driel, J. Sipe, and J. F. Young, "Laser-induced periodic surface structure on solids: A universal phenomenon," *Phys. Rev. Lett.*, vol. 49, p. 1955, 1982.

[2] J. Bonse, J. Krüger, S. Höhm, and A. Rosenfeld, "Femtosecond laser-induced periodic surface structures," *J. Laser Appl.*, vol. 24, 2012, Art no. 042006.

[3] J. Bonse, A. Rosenfeld, and J. Krüger, "On the role of surface plasmon polaritons in the formation of laser-induced periodic surface structures upon irradiation of silicon by femtosecond-laser pulses," *J. Appl. Phys.*, vol. 106, p. 104910, 2009.

[4] M. Rohloff, S. Das, S. Höhm, et al., "Formation of laser-induced periodic surface structures on fused silica upon multiple cross-polarized double-femtosecond-laser-pulse irradiation sequences," *J. Appl. Phys.*, vol. 110, 2011, Art no. 014910.

[5] A. Vorobyev, V. Makin, and C. Guo, "Periodic ordering of random surface nanostructures induced by femtosecond laser pulses on metals," *J. Appl. Phys.*, vol. 101, 2007, Art no. 034903.

[6] A. Y. Vorobyev and C. Guo, "Direct femtosecond laser surface nano/microstructuring and its applications," *Laser Photonics Rev.*, vol. 7, pp. 385–407, 2013.

[7] J. Yao, C. Zhang, H. Liu, et al., "Selective appearance of several laser-induced periodic surface structure patterns on a metal surface using structural colors produced by femtosecond laser pulses," *Appl. Surf. Sci.*, vol. 258, pp. 7625–7632, 2012.

[8] J. Bonse, S. Höhm, A. Rosenfeld, and J. Krüger, "Sub-100 nm laser-induced periodic surface structures upon irradiation of titanium by Ti: sapphire femtosecond laser pulses in air," *Appl. Phys. A*, vol. 110, pp. 547–551, 2013.

[9] C. S. Nathala, A. Ajami, A. A. Ionin, et al., "Experimental study of fs-laser induced sub-100 nm periodic surface structures on titanium," *Opt. Express*, vol. 23, pp. 5915–5929, 2015.

[10] S. Makarov, A. Tsypkin, T. Voytova, et al., "Self-adjusted all-dielectric metasurfaces for deep ultraviolet femtosecond pulse generation," *Nanoscale*, vol. 8, pp. 17809–17814, 2016.

[11] J. Yao, C. Zhang, H. Liu, et al., "High spatial frequency periodic structures induced on metal surface by femtosecond laser pulses," *Opt. Express*, vol. 20, pp. 905–911, 2012.

[12] J. Bonse, M. Munz, and H. Sturm, "Structure formation on the surface of indium phosphide irradiated by femtosecond laser pulses," *J. Appl. Phys.*, vol. 97, 2005, Art no. 013538.

[13] J. Sipe, J. F. Young, J. Preston, and H. Van Driel, "Laser-induced periodic surface structure. I. Theory," *Phys. Rev. B*, vol. 27, p. 1141, 1983.

[14] X.-F. Li, C.-Y. Zhang, H. Li, Q.-F. Dai, S. Lan, and S.-L. Tie, "Formation of 100 nm periodic structures on a titanium surface by exploiting the oxidation and third harmonic generation induced by femtosecond laser pulses," *Opt. Express*, vol. 22, pp. 28086–28099, 2014.

[15] L. Jiang, A.-D. Wang, B. Li, T.-H. Cui, and Y.-F. Lu, "Electrons dynamics control by shaping femtosecond laser pulses in micro/nanofabrication: modeling, method, measurement and application," *Light Sci. Appl.*, vol. 7, p. 17134, 2018.

[16] K. Xiong, D. Tordera, M. P. Jonsson, and A. B. Dahlin, "Active control of plasmonic colors: emerging display technologies," *Rep. Prog. Phys.*, vol. 82, 2019, Art no. 024501.

[17] X. M. Goh, Y. Zheng, S. J. Tan, et al., "Three-dimensional plasmonic stereoscopic prints in full colour," *Nat. Commun.*, vol. 5, p. 5361, 2014.

[18] A. Kristensen, J. K. Yang, S. I. Bozhevolnyi, et al., "Plasmonic colour generation," *Nat. Rev. Mater.*, vol. 2, pp. 1–14, 2016.

[19] M. Yan, J. Dai, and M. Qiu, "Lithography-free broadband visible light absorber based on a mono-layer of gold nanoparticles," *J. Opt.*, vol. 16, 2014, Art no. 025002.
[20] X. Wang, A. Kuchmizhak, D. Storozhenko, S. Makarov, and S. Juodkazis, "Single-step laser plasmonic coloration of metal films," *ACS Appl. Mater. Interfaces*, vol. 10, pp. 1422–1427, 2018.
[21] P. C. Wu, W.-Y. Tsai, W. T. Chen, et al., "Versatile polarization generation with an aluminum plasmonic metasurface," *Nano Lett.*, vol. 17, pp. 445–452, 2016.
[22] L. Deng, J. Deng, Z. Guan, et al., "Malus-metasurface-assisted polarization multiplexing," *Light Sci. Appl.*, vol. 9, pp. 1–9, 2020.
[23] L. Duempelmann, D. Casari, A. Luu-Dinh, B. Gallinet, and L. Novotny, "Color rendering plasmonic aluminum substrates with angular symmetry breaking," *ACS Nano*, vol. 9, pp. 12383–12391, 2015.
[24] J. Olson, A. Manjavacas, L. Liu, et al., "Vivid, full-color aluminum plasmonic pixels," *Proc. Natl. Acad. Sci. U. S. A.*, vol. 111, pp. 14348–14353, 2014.
[25] O. Wilson, G. J. Wilson, and P. Mulvaney, "Laser writing in polarized silver nanorod films," *Adv. Mater.*, vol. 14, pp. 1000–1004, 2002.
[26] Z. Li, A. W. Clark, and J. M. Cooper, "Dual color plasmonic pixels create a polarization controlled nano color palette," *ACS Nano*, vol. 10, pp. 492–498, 2016.
[27] T. D. James, P. Mulvaney, and A. Roberts, "The plasmonic pixel: large area, wide gamut color reproduction using aluminum nanostructures," *Nano Lett.*, vol. 16, pp. 3817–3823, 2016.
[28] L. Zhu, J. Kapraun, J. Ferrara, and C. J. Chang-Hasnain, "Flexible photonic metastructures for tunable coloration," *Optica*, vol. 2, pp. 255–258, 2015.
[29] J. S. Lee, J. Y. Park, Y. H. Kim, et al., "Ultrahigh resolution and color gamut with scattering-reducing transmissive pixels," *Nat. Commun.*, vol. 10, pp. 1–9, 2019.
[30] J. Xiang, J. Li, Z. Zhou, et al., "Manipulating the orientations of the electric and magnetic dipoles induced in silicon nanoparticles for multicolor display," *Laser Photon. Rev.*, vol. 12, p. 1800032, 2018.
[31] Y. Nagasaki, M. Suzuki, and J. Takahara, "All-dielectric dual-color pixel with subwavelength resolution," *Nano Lett.*, vol. 17, pp. 7500–7506, 2017.
[32] F. Z. Shu, F. F. Yu, R. W. Peng, et al., "Dynamic plasmonic color generation based on phase transition of vanadium dioxide," *Adv. Opt. Mater.*, vol. 6, p. 1700939, 2018.
[33] M. A. Kats, R. Blanchard, S. Ramanathan, and F. Capasso, "Thin-film interference in lossy, ultra-thin layers," *Opt. Photonics News*, vol. 25, p. 40, 2014.
[34] M. A. Kats, R. Blanchard, P. Genevet, and F. Capasso, "Nanometre optical coatings based on strong interference effects in highly absorbing media," *Nat. Mater.*, vol. 12, p. 20, 2013.
[35] P. Mao, C. Liu, F. Song, M. Han, S. A. Maier, and S. Zhang, "Manipulating disordered plasmonic systems by external cavity with transition from broadband absorption to reconfigurable reflection," *Nat. Commun.*, vol. 11, pp. 1–7, 2020.
[36] T. Ding, J. Mertens, A. Lombardi, O. A. Scherman, and J. J. Baumberg, "Light-directed tuning of plasmon resonances via plasmon-induced polymerization using hot electrons," *ACS Photonics*, vol. 4, pp. 1453–1458, 2017.
[37] Y. Wang, S. Wang, S. Zhang, et al., "Plasmon-directed polymerization: regulating polymer growth with light," *Nano Res.*, vol. 11, pp. 6384–6390, 2018.
[38] M. M. Ito, A. H. Gibbons, D. Qin, et al., "Structural colour using organized microfibrillation in glassy polymer films," *Nature*, vol. 570, pp. 363–367, 2019.
[39] J. Hao, J. Wang, X. Liu, W. Padilla, L. Zhou, and M. Qiu, "High performance optical absorber based on a plasmonic metamaterial," *Appl. Phys. Lett.*, vol. 96, p. 251104, 2010.
[40] A. Roberts, S. Novikov, Y. Yang, et al., "Laser writing of bright colors on near-percolation plasmonic reflector arrays," *ACS Nano*, vol. 13, pp. 71–77, 2018.
[41] D. Hu, Y. Lu, Y. Cao, et al., "Laser-splashed three-dimensional plasmonic nanovolcanoes for steganography in angular anisotropy," *ACS Nano*, vol. 12, pp. 9233–9239, 2018.
[42] T. Maurer, P. Adam, and G. Lévêque, "Coupling between plasmonic films and nanostructures: from basics to applications," *Nanophotonics*, vol. 4, pp. 363–382, 2015.
[43] S. V. Makarov, V. A. Milichko, I. S. Mukhin, et al., "Controllable femtosecond laser induced dewetting for plasmonic applications," *Laser Photonics Rev.*, vol. 10, pp. 91–99, 2016.
[44] F. Yue, C. Zhang, X.-F. Zang, et al., "High-resolution grayscale image hidden in a laser beam," *Light Sci. Appl.*, vol. 7, p. 17129, 2018.
[45] J. Deng, L. Deng, Z. Guan, et al., "Multiplexed anticounterfeiting meta-image displays with single-sized nanostructures," *Nano Lett.*, vol. 20, pp. 1830–1838, 2020.
[46] J. Ye, D. Zuev, and S. Makarov, "Dewetting mechanisms and their exploitation for the large-scale fabrication of advanced nanophotonic systems," *Int. Mater. Rev.*, vol. 64, pp. 439–477, 2019.
[47] H. Cheng, X. Wei, P. Yu, et al., "Integrating polarization conversion and nearly perfect absorption with multifunctional metasurfaces," *Appl. Phys. Lett.*, vol. 110, p. 171903, 2017.
[48] S. Link, C. Burda, B. Nikoobakht, and M. A. El-Sayed, "Laser-induced shape changes of colloidal gold nanorods using femtosecond and nanosecond laser pulses," *J. Phys. Chem. B*, vol. 104, pp. 6152–6163, 2000.

Supplementary Material: The online version of this article offers supplementary material (https://doi.org/10.1515/nanoph-2020-0651).